Mechanical Systems and Signal Processing 25 (2011) 1073–1085

Contents lists available at ScienceDirect

Mechanical Systems and Signal Processing

journal homepage: www.elsevier.com/locate/jnlabr/ymssp

Identification of micro-vibro-impacts at boundary condition of a nonlinear beam

Hassan Jalali [a,*], Hamid Ahmadian [b], Fatemeh Pourahmadian [b]

[a] Iran University of Science and Technology, Arak Branch, Arak, Iran
[b] Center of Excellence in Solid Mechanics and Dynamics, Iran University of Science and Technology, Tehran, Iran

ARTICLE INFO

Article history:
Received 27 December 2009
Received in revised form
3 September 2010
Accepted 4 September 2010
Available online 15 September 2010

Keywords:
Nonlinear boundary condition
Micro-vibro-impact
Frictional slip

ABSTRACT

Under high amplitude vibrations, contact interfaces experience micro-vibro-impacts and frictional slips. These nonlinear mechanisms can introduce response nonlinearity and energy dissipation into the structures containing them. Beams are widely used in engineering structures and almost in every application they are subjected to boundary conditions. Boundary conditions may contain nonlinear contact interfaces. Therefore, modeling accurately the micro-vibro-impacts and frictional slips developing at the boundary condition of a beam is important in structural dynamics. Ignoring this may result in major discrepancies between experimental observations and theoretical calculations. In this paper identification of micro-vibro-impacts and frictional slips at boundary condition of a nonlinear beam is considered. The structure, being modeled as an Euler–Bernoulli beam, is analyzed using nonlinear normal modes. A reduced-order model governing the dynamic response of the beam near its first resonant point is resulted from the analysis. Identification of the nonlinear boundary condition parameters can be performed by means of the reduced order model and using experimental results.

1. Introduction

Beams are one of the most commonly used elements in mechanical structures. They usually contain boundary conditions of different types. Boundary conditions can cause nonlinearity in the response and dissipation of the energy due to nonlinear mechanisms developing at their contact interfaces. Neglecting the nonlinear characteristics of the boundary conditions is the main source of discrepancies between experimental observations and the results obtained by using analytical/numerical models.

The nonlinear nature of the contact interfaces can be associated to two different mechanisms: slip and slap (or vibro-impact) mechanisms. Slip takes place when two adjacent surfaces, being in contact with each other, move tangentially against each other due to applying an external tangential load. In this condition the interface may experience stick, micro-slip or macro-slip; depending on the amplitude of the applied load. In micro-slip, small regions at the interface area start to slip. Increasing gradually the amplitude of the applied load will result in increasing the size of the micro-slip regions. Finally all the interface area start to slip and the so-called gross or macro-slip happens. Slip mechanism introduces nonlinearity in stiffness and damping characteristics of the contact interface. Precise structural dynamic analysis needs this mechanism to be modeled accurately.

* Corresponding author. Fax: +98 861 38181 41167.
E-mail address: jalali@iust.ac.ir (H. Jalali).

0888-3270/$ - see front matter © 2010 Elsevier Ltd. All rights reserved.
doi:10.1016/j.ymssp.2010.09.007

Comprehensive investigations of friction in contact interfaces have been presented by Ferri [1], Berger [2] and Ibrahim and Pettit [3]. Over past decades, a number of models have been proposed addressing the frictional slip mechanism. Iwan model [4] consists of an array of parallel springs in series with Coulomb friction elements. Dahl model [5] is essentially Coulomb friction but there is a lag in the change of friction force when the direction of motion is changed. The Valanis model [6,7], the Leuven model [8,9] and bristle models [10] are other examples of friction models. These models offer smooth transition from stick to micro-slip and macro-slip (sliding) behavior. Bristle models capture both the micro-slip and macro-slip regimes of interfacial friction. The LuGre friction model [11] is also based on a bristle interpretation of the frictional interface. The above models have been widely used by many researchers for constructing mathematical representations of the structures containing frictional interfaces such as joints. Gaul and Nitsche [12] and Segalman [13] described a range of constitutive and phenomenological models for joint interface mechanisms.

Slap (or vibro-impact) mechanism takes place in contact interfaces which are subjected to high amplitude vibrations. Vibro-impacts develop when nearby portions of the contact interface move against each other in a direction normal to the tangential direction. If the nearby portions completely separate from each other and come to contact repeatedly, macro-vibro-impact happens. The main feature of macro-vibro-impact is transferring energy to higher frequencies than those excite the impact mechanism. Micro-vibro-impacts develop when the applied external loads are less than the interface normal force. In this condition microscopic impacts develop between the elastic deformations and absorb a small amount of energy. The main feature of this mechanism is dissipating energy from the structure in a nonlinear fashion. A comprehensive literature survey on contact dynamics has been presented by Gilardi and Sharf [14].

Impacts developing in the contact interfaces represent a very common source of structural nonlinearity. Modeling and analysis of systems with vibro-impact nonlinearities is a challenging problem in structural dynamics. The effects of vibro-impact (micro and macro) on the dynamics of beams have been the subject of many researches in the past. Emaci et al. [15] studied the nonlinear motion of a flexible assembly consisting of two cantilever beams whose motions were constrained by barriers. They expressed the impact damping in the form of viscous damping (damping proportional to velocity). Moon and Shaw [16] investigated the chaotic behavior of a clamped beam both numerically and experimentally. They assumed that the other end of the beam freely moved in one direction but in the other direction encountered a stop. Knudsena and Massih [17] studied the dynamics of the beams which were clamped at one end and constrained against unilateral contact sites near the other end. They employed Euler–Bernoulli beam theory and Rayleigh damping theory for modeling the structure. The existent and stability of periodic orbits and the local bifurcation under harmonic excitation forces were studied by using Poincare mapping. They verified their approach by using the test results presented by Moon and Shaw [16].

Azeez and Vakakis [18] used proper orthogonal decomposition (POD), also known as the Karhunen–Loeve (K–L) method, to study the nonlinear effects of vibro-impacts on the dynamics of a clamped beam and a rotor. Rigid barriers were used to induce symmetrical vibro-impacts close to the free end of these structures. Kerschen et al. [19] identified a symmetrical and asymmetrical nonlinear beam by using restoring force surface method. The beam was clamped at one end and subjected to rigid barriers – single and double – somewhere in the middle. They used bilinear spring and viscous damping elements and modeled the vibro-impact mechanism. By measuring the beam's response to a harmonic excitation, the parameters of the vibro-impact model were identified.

As it was stated earlier in this section, the main feature of micro-vibro-impact mechanism is to dissipate energy in a nonlinear fashion. This subject has also been investigated by many researchers. Crawley et al. [20] attempted to use the coefficient of restitution to measure the energy dissipation due to impact. Hunt and Crossley [21] showed that the linear damping model does not correctly capture the energy dissipation due to vibro-impacts. They proposed a nonlinear damping model based on the Hertz's theory. Their model was an extension of the model had previously been proposed by Dubowsky and Freudenstein [22]. Dubowsky and Freudenstein used a viscous damping model for representing the energy dissipation of the impact mechanism in the contact interfaces. Many researchers have reported that the impact damping model proposed by Hunt and Crossley can represent the nature of the energy dissipation in the contact interfaces with an acceptable accuracy. The reader is referred to Veluswami et al. [23,24], Azar and Crossley [25] and Padmanabhan and Singh [26] for more details.

To date, impacts developing in the contact interface of joints and boundary conditions have remained an area with very limited investigations. Ma et al. [27] experimentally investigated the vibro-impacts developing in the contact interface of a loose bolted joint. Felkman et al. [28] considered the nonlinearity in the interface of a pinned joint of a truss. They concluded that the main mechanisms developing in the joint interface are friction and impacting. They identified these mechanisms by using experimental results. Based on the best knowledge of the authors, up to date, there is no published article addressing the effects of vibro-impacts on the frictional slip mechanism when they develop simultaneously in a contact interface. In other words, when slip and vibro-impact mechanisms develop simultaneously, the vibro-impacts change the actual normal force of the contact interface. Since the behavior of the slip mechanism depends to this normal force, the slip and vibro impact mechanisms are not decoupled. In these circumstances, the effect of vibro-impacts on the slip mechanism should be considered. This issue is covered in this paper.

The present paper considers identification of micro-vibro-impact and frictional slip mechanisms developing at the boundary condition of a clamped beam. The paper goes as follows: In Section 2 the mathematical model of the structure is constructed using Euler–Bernoulli beam theory. The effects of vibro-impact and slip mechanisms are included using time-dependent functions. The model is analyzed by employing nonlinear normal modes and a reduced order model is obtained

for the structure. Section 3 describes an experimental case study. Using the experimental results and the reduced order model, the equivalent linear system, nonlinear normal modes and the nonlinear contact interface are identified, respectively, in Sections 4 and 5. Finally, the conclusion is drawn in Section 6.

2. Problem formulation and solution

The Euler–Bernoulli cantilever beam considered in this paper has a contact boundary condition at $x=L$, where x is the spatial co-ordinate (see Fig. 1). The beam is characterized by E as Young's modulus, I the cross-sectional moment of inertia, ρ the density, A the cross-sectional area and L the length. The distance between contact point and beam's neutral axis is denoted by z_0. A constant normal force P is applied to the beam at $x=L$. The beam is excited into forced vibration using a harmonic force, i.e. $F(t)=f\sin(\omega t)$. The single point excitation is applied at location $x=D$. The lateral deflection of the beam is denoted by $w(x,t)$.

It is assumed that the contact point is not rigid and small deflections at this point are permitted. Therefore the dynamic response of the beam is affected by the way that the contact point behaves. At low amplitude vibrations, the contact point is in stick condition in the tangential direction (x direction) and in the normal direction (w direction) the applied normal force P prevents lateral movements. At these circumstances the structure behaves linearly. If the amplitude of vibrations is increased, micro-slip and micro-vibro-impact develop in the contact interface due to the rotation and lateral movement of the beam end. These two mechanisms are inherently nonlinear and introduce nonlinearity in the dynamic response of the beam. The contribution of this paper is, first, to address the effects of micro-vibro-impacts on the frictional slip mechanism when they develop simultaneously in a contact interface and, second, to identify these mechanisms by using experimental results. In the following, the effect of these mechanisms on the dynamic response of the structure shown in Fig. 1 is mathematically explored. The identification will be considered in next sections.

Micro-slip and micro-vibro-impact mechanisms exert dynamic forces to the beam end. The effects of these mechanisms are considered in this paper by using time-dependent forces $N(t)$ and $R(t)$, respectively, for slip and impact mechanisms. The direction of these forces is shown in Fig. 2. By using Figs. 1 and 2, one may obtain the equation governing the lateral deflection of the beam as

$$\rho A\ddot{w}+EIw''''-N(t)w''=F(t)\delta(x-D) \tag{1}$$

where $(\bullet)$ denotes derivation with respect to time variable t and $(\ )'$ denotes derivation with respect to spatial variable x. The friction force $N(t)$, being moved to the neutral axis, imposes an axial force to the beam. Eq. (1) also considers the effect of this axial force on lateral deflection. Eq. (1) is subjected to the following boundary conditions corresponding to the clamped end of the beam

$$w(0,t)=0,\quad w'(0,t)=0, \tag{2,3}$$

Eqs. (2) and (3) show the conditions imposing by the clamped end on the displacement and slope of the beam. At the right end, the boundary conditions are

$$EIw''(L,t)=z_0N(t),\quad EIw'''(L,t)=F_n(t)+m\ddot{w}(L,t) \tag{4,5}$$

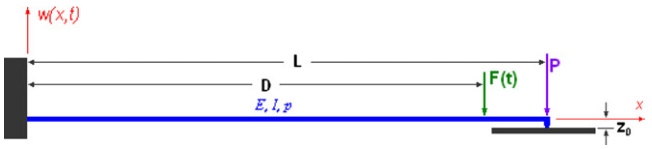

Fig. 1. Euler–Bernoulli beam with contact boundary condition.

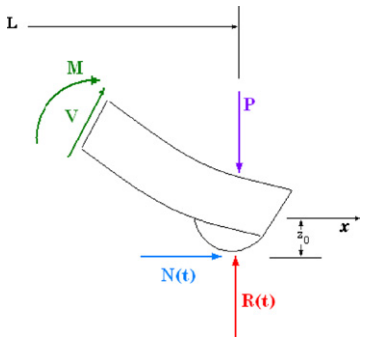

Fig. 2. Direction of the slip and impact forces at the contact point.

Left-hand side of Eq. (4) is the bending moment of the beam corresponding to the contact point. This moment is equal to the couple moment created by moving friction force $N(t)$ to the neutral axis. Eq. (5) describes the shearing force of the beam at $x=L$. The right-hand side of this equation is composed of two terms. The first term is $F_n(t)=R(t)-P$, i.e. the actual normal force applied to the contact interface. The second term needs explanations: in the experimental section, it will be described that the normal force P is exerted to the contact interface by using a set of blocks of mass m. The second term in right-hand side of Eq. (5) shows the inertia force of the blocks.

In above equations, $N(t)$ and $R(t)$ are functions of, respectively, shear deformation and velocity, i.e. $u(t)$, $\dot{u}(t)$ and lateral deformation and velocity, i.e. $w(L,t)$, $\dot{w}(L,t)$, corresponding to the contact point. Shear deformation of the contact point results from the lateral motion of the beam and can be expressed as Eq. (6). The first term in Eq. (6) corresponds to the shortening of the beam length due to its lateral motion, the second term results from rotation of the beam end and the third term is attributed to axial deformation due to frictional force $N(t)$

$$u(t)=-\frac{1}{2}\int_0^L\left(\frac{\partial w(x,t)}{\partial x}\right)^2 dx+r\frac{\partial w(L,t)}{\partial x}+N(t)L/AE \tag{6}$$

Eq. (6) indicates that $u(t)$ depends on $w(L,t)$; which means that micro-vibro-impact and frictional slip mechanisms are coupled.

The governing equation and boundary conditions, Eqs. (1–6), are nonlinear as they contain micro-slip and micro-vibro-impact forces, i.e. $N(t)$ and $R(t)$, which are nonlinear functions. Before solving these equations, first the models being used in this paper for representing slip and impact mechanisms are described in following.

From the various models which have been presented in the literature for modeling frictional slip, three have gained more attention in structural dynamics: Iwan, LuGre and Valanis models. Iwan model [4] consists of an array of parallel springs in series with Coulomb friction elements—the so called Jenkins elements. When one Jenkins element, i.e. one spring in series with one friction element, is used to model the frictional contact interface, the frictional slip model displays bilinear properties which indicate that there is an abrupt transition from stick to slip regime. This is not in consistent with what is observed in reality where the transition from stick to slip is smooth. One alternative way to solve this problem is using an array of parallel Jenkins elements. The Jenkins elements then have the same stiffness coefficient but breaking away force of friction elements is different. In Iwan model a probabilistic distribution function governs the breaking away force of friction elements. The Iwan and LuGre model have more physical insight than the Valanis model. The advantage of the Valanis model over the other two models is that this model needs fewer parameters to define the frictional contact interface. In the following, the LuGre and Valanis models, which will be used in this paper, are described in more details.

The LuGre model presented by Wit et al. [11] captures a verity of behaviors such as hysteresis effects and pre-sliding displacement. This six parameter model is based on the bristle interpretation of the contact interface and its friction force is defined as

$$N(t)=(\sigma_0 z(t)+\sigma_1\dot{z}(t)+\sigma_2\dot{u}(t))P \tag{7}$$

$$\dot{z}(t)=\dot{u}(t)-\sigma_0 z(t)|\dot{u}(t)|/g(\dot{u}) \tag{8}$$

$$\sigma_0 g(\dot{u})=\mu_c+(\mu_s-\mu_c)e^{-|\dot{u}(t)/v_s|^2} \tag{9}$$

where σ_0 is the average bristle stiffness, σ_1 the damping parameter and σ_2 accounts for the viscous damping. μ_c and μ_s are, respectively, Coulomb and static friction coefficients, v_s the Stribeck velocity and P the contact normal force.

The four parameter Valanis model was adopted from the theory of elasticity [6,7]. In this model, the change of the friction force, $N(t)$, is given by the following equation:

$$\dot{N}(t)=\frac{e_0\dot{u}\left[1+\frac{\lambda}{e_0}\mathrm{sgn}(\dot{u})(e_t u-N(t))\right]}{1+\kappa\frac{\lambda}{e_0}\mathrm{sgn}(\dot{u})(e_t u-N(t))},\quad \lambda=\frac{e_0}{\alpha_0\left(1+\kappa\frac{e_t}{e_0}\right)} \tag{10}$$

where e_0 is the stiffness modulus of contact interface at sticking condition, e_t shows the slope of the slip motion, κ controls the smoothness of the hysteresis loop for transition from stick to slip and λ is characterized by the stick limit.

The model presented by Hunt and Crossley [21] is used in this paper for taking into account the effects of micro-vibro-impacts. This model, which is based on interpretation of impact damping by using coefficient of restitution, consists of a linear spring and a nonlinear damping. It was proposed by Hunt and Crossley for describing impacts between compact solid bodies. When the bodies are in compressive contact and there is no backlash in the interface, microscopic impacts develop between the elastic deformations and thereby absorb a small amount of energy. In this condition the contact normal force can be expressed as

$$R(t)=w(L,t)(\alpha+\beta\dot{w}(L,t)) \tag{11}$$

where α and β represent, respectively, the stiffness and damping characteristics of contact interface in normal direction.

Up to this point, the governing equation and boundary conditions of the structure shown in Fig. 1 were derived. Also, three models were described which will be used in later sections when identification of the micro-slip and

micro-vibro-impact mechanisms is considered. In the following a solution is given for the above stated problem which is useful for identification purposes.

The dynamic response of a structure is more affected by the boundary conditions in the lower modes. On the other side, the behavior of the slip and micro-vibro-impact mechanisms is frequency independent. Keeping these in mind, in this study, the external excitation force $F(t)$ is considered single harmonic and the excitation frequency is chosen to be close to the first resonant point. Therefore, the nonlinear behavior of the beam can be spanned using its first n nonlinear normal modes $\{\omega_i(a),\tilde{\phi}_i(x,a)\}$ as

$$w(x,t)=\sum_{i=1}^{n}\tilde{\phi}_i(x,a)q_i(t) \tag{12}$$

The nonlinear normal modes are equal to the modes of corresponding linearized structure at the same response amplitude level [29,30]. They are functions of the maximum response amplitude level corresponding to the driving point, i.e. a

$$a=\max\left\{w(D,\bar{t}),\quad \bar{t}\in\left[t,t+\frac{2\pi}{\omega_n}\right]\right\} \tag{13}$$

Substituting Eq. (12) into Eq. (1), multiplying the resultant equation into $\tilde{\phi}_j(x,a)$ and integrating over the beam length and after some algebraic manipulations, the following equation is obtained

$$\ddot{q}_i(t)+\omega_i^2(a)q_i(t)-F(t)\tilde{\phi}_i(D,a)=\left(z_0\tilde{\phi}'_i(L,a)+\sum_{r=1}^{n}q_r(t)\int_0^L\tilde{\phi}''_r(x,a)\tilde{\phi}_i(x,a)dx\right)N(t)-\tilde{\phi}_i(L,a)F_n(t),\quad i=1,2,\ldots,n \tag{14}$$

The details about deriving Eq. (14) are provided in Appendix.

The theory described and the equations derived in this section are used in subsequent sections and the contact shear and normal interface forces, i.e. $N(t)$ and $R(t)$, are characterized. In the following section the results obtained from an experimental case study are presented.

3. Experimental case study

The experimental beam is pictured in Fig. 3. The structural parameters of the beam were given by L=600 mm (length), b=40 mm (width) and h=5 mm (thickness). The beam was clamped at one end and the other end was subjected to a contact boundary condition. The contact boundary condition was provided by a pin welded to the beam end. The pin, 5 mm in radius, was allowed to slip/slap on an underlying steel block as is shown in Fig. 3. Suspended blocks, m=10 kg were used to apply a constant normal force to the contact interface.

The contact interface experiences different behaviors depending on the vibration amplitude level. Under low amplitude vibrations it behaves linearly. As vibration amplitude increases, micro/macro-slip and micro-vibro-impact mechanisms develop and introduce nonlinearity into the response. A point worth to be mentioned about micro-vibro-impacts is that the stiffness of the contact point in normal direction changes when micro-vibro-impacts develop. In fact, when the pin is compressed against the underlying steel block, the stiffness of the steel block plays the role of the stiffness in the normal direction. In contrast, when the pin moves in opposite direction, the flexible wire used for suspending the masses contributes to the stiffness of the contact point. This implies that in normal direction the stiffness of the contact point is bilinear. This will be approved later in this paper by using experimental results.

The structure was excited using a B&K4200 mini shaker attached trough a stinger to the structure at distance S=550 mm, measured from the clamped end. A B&K8200 force transducer was used between stinger and structure in order to measure the excitation force $F(t)$. The structural response was measured using three accelerometers mounted on the beam at locations x_1=550, x_2=300 and x_3=100 mm (all measured from the clamped end). The transducers arrangement is shown in Fig. 3. A low

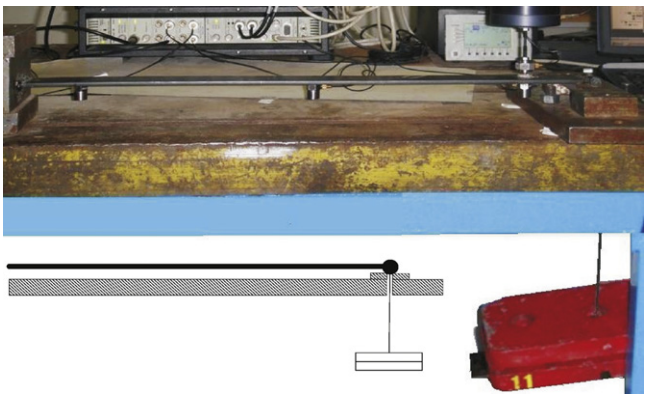

Fig. 3. Test set-up.

level random excitation force was first applied to the structure, ensuring that the contact interface was in stick regime, and the linear FRFs were measured. Fig. 4 shows a typical linear FRF. The frequency response function shown in Fig. 4 has symmetry around the resonant points and no jump is evident; indicating that the contact interface was in stick regime and therefore the structural behavior was linear. In Table 1 the corresponding linear natural frequencies are tabulated.

Next, measurement of the nonlinear FRFs by using constant response amplitude level approach [31] was considered. The structure was excited using a harmonic force and the excitation frequencies were chosen to be close to the first natural frequency. The response amplitude level a corresponding to the driving point was kept constant at all excitation frequencies. The excitation force and response signals were recorded and the nonlinear FRFs were constructed. Fig. 5 shows the obtained nonlinear FRFs corresponding to the driving point in different response amplitude levels.

Although FRFs shown in Fig. 5 look like linear FRFs, which is due to keeping the response amplitude level constant, still the time domain signals, which were recorded at each excitation frequencies, contain nonlinearity effects and can be used in characterization of the contact interface [32]. Two main features of the nonlinear mechanisms developing in the contact interface are evident from Fig. 5: shifting the resonant points to lower frequencies and initially decreasing and then increasing the peak amplitude of FRFs when response amplitude level is increased. The former indicates the softening effect and the later shows displacement dependent damping effect of the contact interface. It will be shown in next sections that the models described in Eqs. (7–11) are well able to capture these effects.

The level of damping in a system can be discerned qualitatively from its FRF. Therefore the damping characteristics of the structure shown in Fig. 3 can be discussed by using the FRFs shown in Figs. 4 and 5. Fig. 4 shows the frequency response

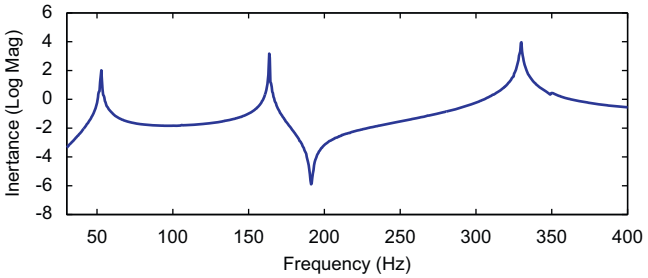

Fig. 4. Linear frequency response function.

Table 1
Experimental and updated natural frequencies (Hz), k_w=302763684.01 (N/m), k_θ=183.91 (Nm/rad).

	Exp.	Upd.	Err. (%)
First mode	52.68	52.69	0.03
Second mode	163.64	162.46	−0.68
Third mode	329.77	323.52	−1.87

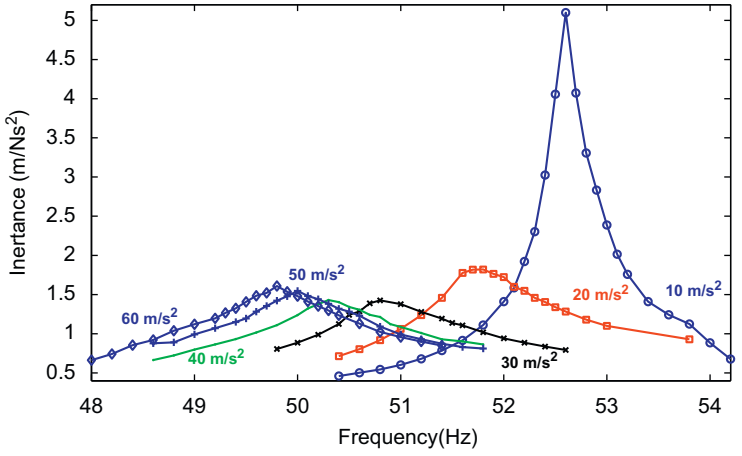

Fig. 5. Nonlinear frequency response functions at different response amplitude levels, 10 m/s^2 (○), 20 m/s^2 (□), 30 m/s^2 (×), 40 m/s^2 (●), 50 m/s^2 (+), 60 m/s^2 (◇).

curve of linear structure. The damping ratio obtained by using this curve corresponds to the beam and not the frictional contact interface. The sharp and narrow peaks at three resonant points in Fig. 4 indicate low material damping of the beam. Also, Fig. 5 shows that when the structure is excited at response amplitude level of 10 m/s^2, the peak of the frequency response curve is still sharp and narrow. At this response amplitude level, the nonlinear mechanisms at the contact interface have not been excited well and the structural behavior is linear. When response amplitude level is increased to 20 m/s^2, the friction damping at the contact interface causes a big decrease in the peak amplitude of the frequency response curve. Therefore comparing the frequency response curves corresponding to 10 and 20 m/s^2 shows that the structural damping is much lower than the friction damping. For these reasons the effect of material damping was ignored in governing equation of system, i.e. Eq. (1).

In Eq. (12) the response was considered to be spanned by nonlinear normal modes. Next section considers identification of the equivalent linear system and calculation of the nonlinear normal modes.

4. Equivalent linear system and nonlinear normal modes

In this section first an equivalent linear system is presented for the nonlinear structure introduced in Eq. (14). Then, by using the experimental results and adopting the equivalent linear system, the nonlinear normal modes are calculated. In order to reduce the order of the model defined in Eq. (14), the nonlinear normal modes of the following system are considered:

$$EIw'''' + \rho A\ddot{w} = 0 \tag{15}$$

$$w(0,t) = 0, \quad w'(0,t) = 0, \quad EIw''(L,t) = k_\theta(a)w'(L,t) \tag{16-18}$$

$$-EIw'''(L,t) = k_w w(L,t) - m\ddot{w}(L,t) \tag{19}$$

$k_\theta(a)$ and k_w represent the flexural and normal stiffness coefficients of the boundary condition, respectively. They are in fact the equivalent linear stiffness of the slip and micro-vibro-impact mechanisms. $k_\theta(a)$ is considered amplitude dependent but k_w is assumed to be constant. This assumption is made based on the fact that the natural frequencies are not sensitive to this parameter. This issue will be covered in details later in this section.

It was stated in previous section that the stiffness of the contact interface in normal direction is bilinear. The position of the change in the stiffness is at $w(L,t)=0$. Such a system is inherently nonlinear but shows homogeneity in frequency domain [33]. Therefore, in Eq. (19) k_w is an equivalent linear stiffness coefficient and is obtained from Eq. (20) [34]

$$k_w = \frac{4\alpha_1\alpha_2}{\left(\sqrt{\alpha_1}+\sqrt{\alpha_2}\right)^2} \tag{20}$$

In Eq. (20), α_1 and α_2 are normal stiffness coefficients of the contact interface in two opposite directions, i.e. when $w(L,t) > 0$ and when $w(L,t) < 0$. These parameters will be identified later in this paper by using time domain experimental results.

Eqs. (15–19) offer a simplified model of the structure where the geometrical stiffness introduced by the friction force in the beam is ignored. This simplified model is an equivalent linear model of the structure and is the model used in identification of the nonlinear normal modes. The effect of the geometrical stiffness of friction force will be considered later when the nonlinear model of the contact interface is characterized.

Having the reduced order model defined by Eqs. (15–19), identification of the linear parameters of the contact interface is considered by employing model updating. There are two parameters, k_w and k_θ, to be identified in updating procedure. These parameters are identified by minimizing the differences between analytical and experimental natural frequencies. The minimization is done by adopting eigen-value sensitivity approach. The analytical natural frequencies are obtained by solving the eigen-value problem of an equivalent FE model corresponding to the beam described by Eqs. (15–19). In the FE model, the mass effects of the accelerometers and force transducer are also considered. The identified parameters, experimental and updated natural frequencies are shown in Table 1.

Next, calculation of the nonlinear normal modes is considered. This needs the equivalent linear system at each response amplitude level to be identified. The equivalent linear system was introduced in Eqs. (15–19). In the experimental section, the FRFs near the first resonant point were presented at different response amplitude level a. Curve fitting these experimental FRFs, the first natural frequency of corresponding linear system can be identified. In Table 2 the amplitude dependent first natural frequencies are tabulated. There remains two parameters, i.e. $k_\theta(a)$ and k_w, to be identified and then the equivalent linear system at each response amplitude level will be known. The mode shapes of these equivalent linear systems are different at different response amplitude levels. These amplitude dependent mode shapes are considered as the nonlinear normal modes. $k_\theta(a)$ and k_w are identified as is explained following.

Sensitivities of the natural frequencies with respect to k_θ and k_w are shown in Table 3. The results presented in this table are obtained by using the identified linear system characterized by the parameters given in Table 1. Table 3 shows that the first natural frequency is not sensitive to k_w. This means, changing k_w does not affect the first natural frequency too much. Therefore k_w is kept constant and is considered to be equal to the value obtained for linear system (Table 1). There remains the flexural stiffness, $k_\theta(a)$, to be identified. This parameter is identified by solving the characteristic equation of linear

Table 2
1st natural frequencies and corresponding contact interface stiffness coefficients.

a, (m/s^2)	$\omega_1(a)$, (Hz)	$k_\theta(a)$, (Nm/rad)
20	51.75	129.74
30	50.81	83.41
40	50.37	61.61
50	50.03	45.36

Table 3
Sensitivities of natural frequencies with respect to k_w and k_θ.

	$\frac{\partial\omega_n^2}{\partial k_w}k_w$	$\frac{\partial\omega_n^2}{\partial k_\theta}k_\theta$
First mode	0.84	1255.31
Second mode	29.00	46343.90
Third mode	226.40	91293.94

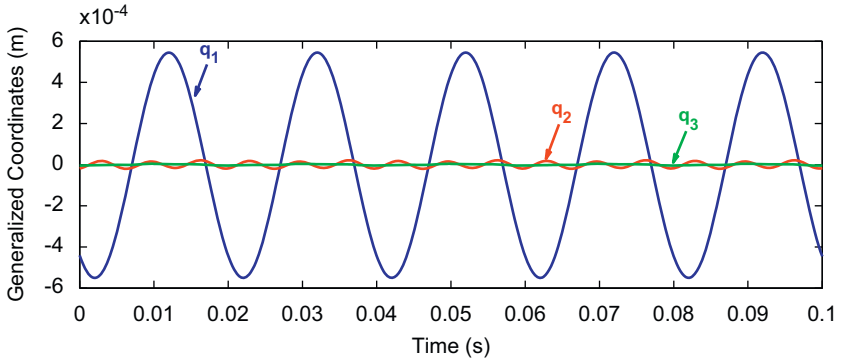

Fig. 6. The generalized coordinated at a=50 m/s^2.

problem defined in Eqs. (15–19). The identified flexural stiffness coefficients at different response amplitude levels, i.e. $k_\theta(a)$, are also tabulated in Table 2. The results presented in Table 2 correspond to those response amplitude levels where the micro-vibro-impacts develop.

The above discussion about k_w being constant can be also verified in the following way. As it was stated earlier in this section, $k_\theta(a)$ and k_w are, respectively, the equivalent linear stiffness coefficients of slip and micro-vibro-impact mechanisms. From Eqs. (11) and (20) it can be deduced that the equivalent linear stiffness of micro-vibro-impact mechanism is constant.

Using the identified equivalent linear system at each response amplitude level, the nonlinear normal modes $\omega_i(a),\tilde{\phi}_i(x,a)$ are obtained. In this paper it is assumed that only the first three normal modes contribute in the dynamic response of the structure as we have employed only three accelerometers in the measurement setup. This assumption is verified in this section by using experimental results. Writing Eq. (12) for each measured responses and employing the nonlinear normal modes calculated in this section, the vector of generalized accelerations, i.e. $\ddot{\mathbf{q}}(t)$, is calculated. By performing integration of this vector twice $\mathbf{q}(\mathbf{t})=[q_1(t),q_2(t),q_3(t)]^T$ is obtained. The harmonic nature of the response signals makes analytical integration possible. Analytical integration is more reliable because it does not suffer from the phased shift which is a problem in numerical integration. In Fig. 6 the generalized coordinates $\mathbf{q}(\mathbf{t})$ are shown at a=50 m/s^2. At this response amplitude level it is expected that the higher modes contribute in the response. Fig. 6 shows that only first and second modes contribute in spanning the structural response and contribution of the third mode is negligible. Therefore the assumption that the first three modes contribute in the dynamic response of the structure is valid. $\mathbf{q}(\mathbf{t})$ and $\ddot{\mathbf{q}}(\mathbf{t})$ are used in next section and the nonlinear contact interface is characterized.

5. Nonlinear contact interface characterization

This section considers characterization of the nonlinear contact interface modeled by nonlinear functions $N(t)$ and $R(t)$ in Eqs. (1–5). In previous section the prerequisites for identification of $N(t)$ and $R(t)$ – i.e. $q_i(t)$, $\ddot{q}_i(t)$and $\omega_i(a),\tilde{\phi}_i(x,a)$ – were calculated. The nonlinear normal modes were obtained by including torsional and lateral effects of virtual stiffness

coefficients $k_\theta(a)$ and k_w in the boundary. These effects need to be addressed in reduced order model by rearrangement of Eq. (14) in the following form:

$$\ddot{q}_i(t)+\omega_i^2(a)q_i(t)-F(t)\tilde{\phi}_i(D,a)-k_\theta(a)\tilde{\phi}'_i(L,a)\left(\sum_{r=1}^{n} q_r(t)\tilde{\phi}'_i(L,a)\right)-k_w\tilde{\phi}_i(L,a)\left(\sum_{r=1}^{n} q_r(t)\tilde{\phi}_r(L,a)\right)$$
$$=\left(\sum_{r=1}^{n} q_r(t)\int_0^L \tilde{\phi}''_r(x,a)\tilde{\phi}_i(x,a)dx-r\tilde{\phi}'_i(L,a)\right)N(t)-\tilde{\phi}_i(L,a)F_n(t),\quad i=1,2,\ldots,n \tag{21}$$

where $F_n(t)=R(t)-P$.

In following the first generalized co-ordinate, i.e. $i=1$, is used and the nonlinear forces $N(t)$ and $R(t)$ are identified. Other co-ordinates lead almost similar results. Also the measurement noise has considerable effects in their results. The LuGre and Valanis models, described by Eqs. (7–10), are used for modeling the frictional force in contact interface. The capability of these models in representing the experimental friction force is investigated in this paper. For modeling micro-vibro-impacts the model proposed by Hunt and Crossley [21], Eq. (11), is used. The parameters of these models are identified as is described following.

By considering a set of parameters for impact model, i.e. Eq. (11), and substituting $w(L,t)$ and $\dot{w}(L,t)$ – known from experimental results – in this equation, $R(t)$ can be obtained. Substituting $R(t)$ in Eq. (21), $N(t)$ is obtained. Using $N(t)$ and employing Eq. (6), $u(t)$ is calculated and by performing differentiation in frequency domain $\dot{u}(t)$ is also known. Having $u(t)$ and $\dot{u}(t)$, $N(t)$ can be regenerated by using Valanis/LuGre model. The parameters of Eq. (11) are fine tuned in a way that the best fit is achieved between $N(t)$ that is regenerated by Valanis/LuGre model and the one obtained from experimental results, i.e. by solving Eq. (21). Fig. 7 shows the identified impact force $R(t)$, and its corresponding parameters are given in Eq. (22)

$$R(t)=\begin{cases}(0.83\times10^8+3.0\times10^{13}\dot{\delta})\delta, & \delta>0\\ (3.6\times10^{10}+2.4\times10^{14}\dot{\delta})\delta, & \delta<0\end{cases} \tag{22}$$

where $\delta=w(L,t)$.

Eq. (22) shows that the stiffness of the contact interface in normal direction is bilinear. The identified stiffness coefficients for $\delta>0$ and $\delta<0$ are such that they satisfy Eq. (20).

The experimental friction force $N(t)$ and the friction force regenerated by fitting the Valanis model, defined by Eq. (10), are shown in Fig. 8. It is worth mentioning that although the external normal force P (see Fig. 1) applied at the boundary condition is constant, the micro-vibro-impacts, developing at the contact interface, change the actual normal force and hence the nature of the slip mechanism. Therefore different Valanis models are obtained at different response amplitude levels. In Table 4 the parameters of Valanis model are tabulated.

In Fig. 9 the experimental friction force $N(t)$ and the friction force regenerated by fitting a LuGre model, Eqs. (7–9), are compared. In fitting the LuGre model the static and dynamic friction coefficients are considered as $\mu_s=0.74$ and $\mu_c=0.57$. These values correspond to steel–steel contact condition. The remaining parameters of the LuGre model at different response amplitude levels are shown in Table 5.

Results presented in Figs. 8 and 9 show that both Valanis and LuGre models are well able to represent the friction force in a contact interface. The effect of the micro-vibro-impacts on frictional slip is investigated in Fig. 10. Fig. 10 shows that when micro-vibro-impact is considered the hysteresis loop shows more symmetry and a better regeneration of the friction force by Valanis model is obtained. In other words, micro-vibro-impact mechanism affects the frictional slip mechanism when they simultaneously develop in a contact interface. The results shown in Fig. 10 correspond to response amplitude level of $a=50$ m/s^2.

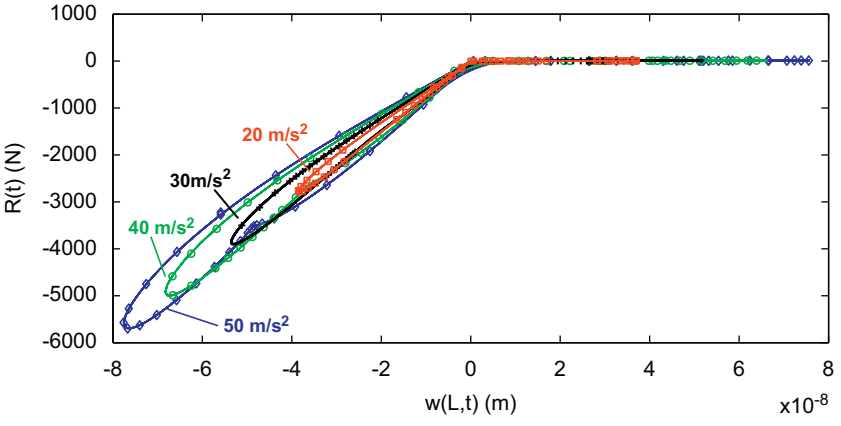

Fig. 7. Identified impact force $R(t)$, 20 m/s^2 (□), 30 m/s^2 (+), 40 m/s^2 (○), 50 m/s^2 (◇).

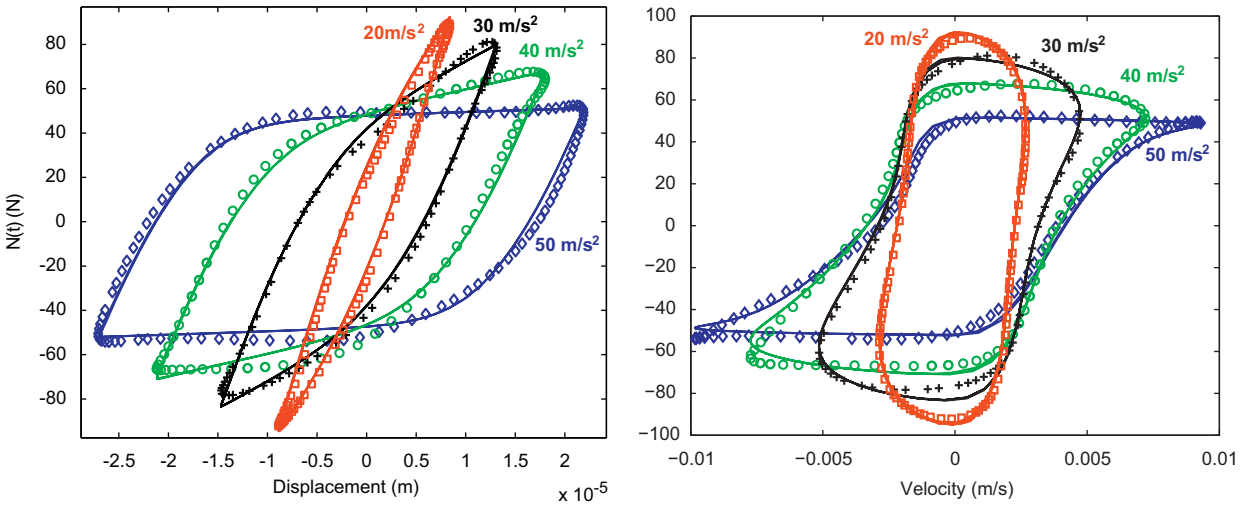

Fig. 8. Experimental (points) and regenerated (lines) friction force $N(t)$, 20 m/s^2 (□), 30 m/s^2 (+), 40 m/s^2 (○), 50 m/s^2 (◇): Valanis model.

Table 4
Parameters of Valanis model, κ=0.5.

a, (m/s^2)	e_0, (MN/m)	e_t, (MN/m)	λ, $\times 10^5$
20	12.8	4.5	1.6
30	9.8	2.3	1.7
40	8.5	1.0	1.6
50	7.8	0.15	1.61

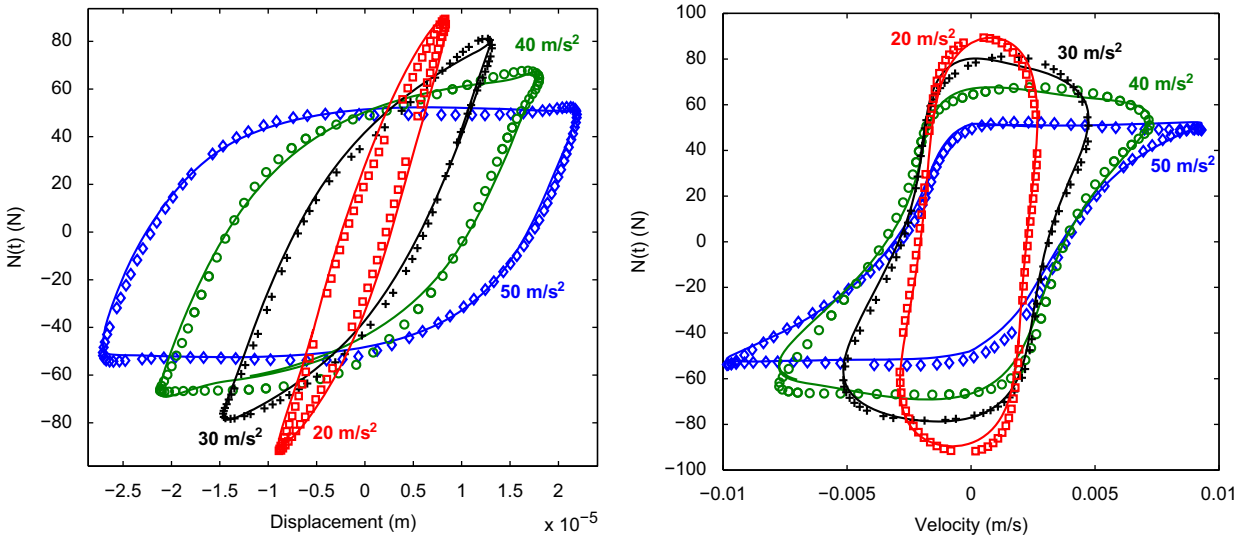

Fig. 9. Experimental (points) and regenerated (lines) friction force $N(t)$, 20 m/s^2 (□), 30 m/s^2 (+), 40 m/s^2 (○), 50 m/s^2 (◇): LuGre model.

Table 5
Parameters of LuGre model.

a, (m/s^2)	σ_0, (MN/m)	σ_1, (Ns/m)	σ_2, (Ns/m)	v_s, (mm/s)
20	11.6	0.03	0.011	4.3
30	7.8	0.05	0.013	3.5
40	6.2	0.08	0.015	3.0
50	5.4	0.11	0.02	2.5

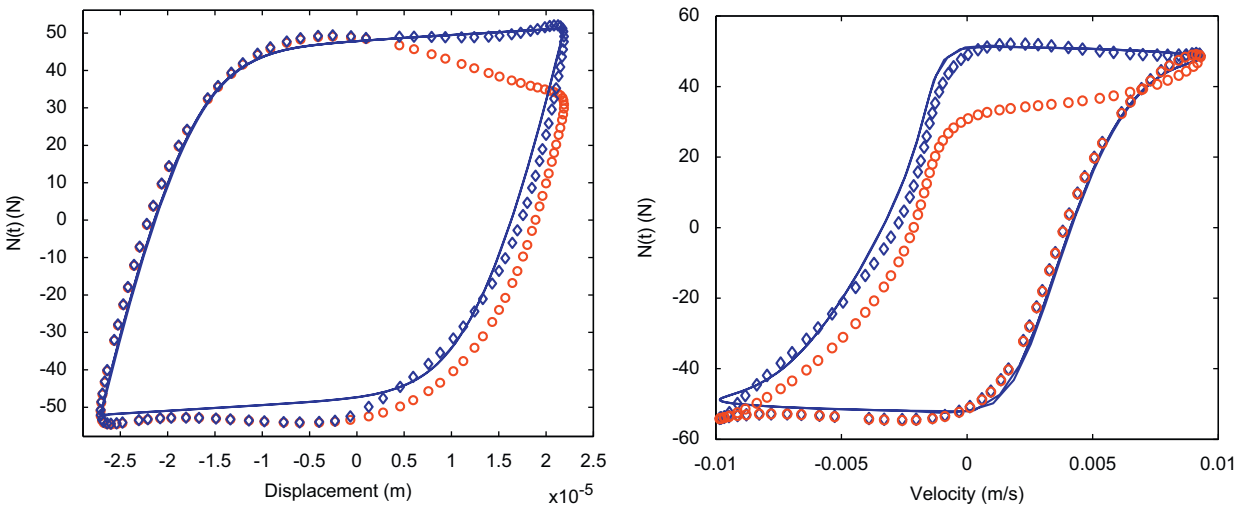

Fig. 10. Experimental hysteresis loops with (◇) and without (○) including micro-vibro-impact effects and the regenerated friction force by Valanis model (lines).

6. Conclusions

Identification of the nonlinear contact interface at the boundary condition of a clamped beam was considered. Small deformations in normal and tangential directions at the contact interface – causing micro-vibro-impacts and frictional slip – were considered and a mathematical model of the structure was developed by using Euler–Bernoulli beam theory. The effects of the slip and micro-vibro-impact mechanisms were included in the mathematical model using nonlinear functions. It was assumed that the slip mechanism is governed by Valanis/LuGre friction models. A model consisting of a linear spring and a displacement dependent viscous damping [21] was considered for representing micro-vibro-impact mechanism. The mathematical model of the structure was then analyzed considering that the response is spanned by nonlinear normal modes. The analysis resulted in a reduced order model governing the dynamic response of the structure near its first natural frequency. Experiments were performed on the real structure and the nonlinear FRFs were measured using constant response amplitude approach. Using the FRFs it was shown that the material damping of the beam is negligible. Therefore its effect was not considered in the mathematical model of the structure. In order to calculate the nonlinear normal modes, the functions governing the slip and micro-vibro-impact mechanisms were replaced by the corresponding equivalent linear stiffness of these mechanisms and an equivalent linear model was proposed for the structure. Using the experimental FRFs, different equivalent linear systems were identified at different response amplitude levels. The mode shapes of these equivalent linear systems, which are displacement dependent, were considered as nonlinear normal modes. Using the calculated nonlinear normal modes at each response amplitude level and the time domain signals measured in the experiments, the parameters of the models considered for slip and micro-vibro-impact mechanisms were identified. The experimental hysteresis loops and those obtained by using identified models were in a good agreement. This indicates that both Valanis and LuGre models are well able to represent the friction force in a contact interface. Based on the results obtained, it was concluded that micro-vibro-impact mechanism affects the frictional slip mechanism when they simultaneously develop in a contact interface.

Appendix

By substituting Eq. (12) into Eqs. (1–5) one may obtain

$$EI\sum_{i=1}^{n} q_i(t)\tilde{\phi}_i''''(x,a) - N(t)\sum_{i=1}^{n} q_i(t)\tilde{\phi}_i''(x,a) + \rho A\sum_{i=1}^{n}\ddot{q}_i(t)\tilde{\phi}_i(x,a) = F(t)\delta(x-D) \tag{A1}$$

$$\sum_{i=1}^{n} q_i(t)\tilde{\phi}_i(0,a) = 0, \quad \sum_{i=1}^{n} q_i(t)\tilde{\phi}'_i(0,a) = 0, \quad EI\sum_{i=1}^{n} q_i(t)\tilde{\phi}_i''(L,a) = z_0 N(t) \tag{A2–A4}$$

$$EI\sum_{i=1}^{n} q_i(t)\tilde{\phi}_i'''(L,a) = F_n(t) + m\sum_{i=1}^{n}\ddot{q}_i(t)\tilde{\phi}_i(L,a) \tag{A5}$$

Multiplying Eq. (A1) into $\tilde{\phi}_j(x,a)$ and integrating over the beam length, results in

$$\left(EI\sum_{i=1}^{n} q_i(t)\int_0^L \tilde{\phi}_i''''(x,a)\tilde{\phi}_j(x,a)\right)-\left(N(t)\sum_{i=1}^{n} q_i(t)\int_0^L \tilde{\phi}_i''(x,a)\tilde{\phi}_j(x,a)\right)+\left(\rho A\sum_{i=1}^{n}\ddot{q}_i(t)\int_0^L \tilde{\phi}_i(x,a)\tilde{\phi}_j(x,a)\right)=F(t)\tilde{\phi}_j(D,a) \tag{A6}$$

Carrying out the double integration part by part to the first term of Eq. (A6) and using the boundary conditions of Eqs. (A2–A5) results in the following equation:

$$\sum_{i=1}^{n}\left[\ddot{q}_i(t)\left(\rho A\int_0^L \tilde{\phi}_i(x,a)\tilde{\phi}_j(x,a)dx+m\tilde{\phi}_i(L,a)\tilde{\phi}_j(L,a)\right)+q_i(t)\left(EI\int_0^L \tilde{\phi}_i''(x,a)\tilde{\phi}_j''(x,a)dx\right)\right]$$
$$-F(t)\tilde{\phi}_j(D,a)=\left(z_0\tilde{\phi}'_j(L,a)+\sum_{i=1}^{n} q_i(t)\int_0^L \tilde{\phi}_i''(x,a)\tilde{\phi}_j(x,a)dx\right)N(t)-\tilde{\phi}_j(L,a)F_n(t) \tag{A7}$$

By using the orthogonality condition, Eq. (A7) finally is simplified to Eq. (14). The used orthogonality conditions are

$$\rho A\int_0^L \tilde{\phi}_i(x,a)\tilde{\phi}_j(x,a)dx+m\tilde{\phi}_i(L,a)\tilde{\phi}_j(L,a)=\delta_{ij} \tag{A8}$$

$$EI\int_0^L \tilde{\phi}_i''(x,a)\tilde{\phi}_j''(x,a)dx=\omega_i^2\delta_{ij} \tag{A9}$$

References

[1] A.A. Ferri, Friction damping and isolation systems, Journal of Mechanical Design 117 (1995) 196–206.
[2] E.J. Berger, Friction modeling for dynamic system simulation, Applied Mechanics Reviews 55 (2002) 535–577.
[3] R.A. Ibrahim, C.L. Pettit, Uncertainties and dynamic problems of bolted joints and other fasteners, Journal of Sound and Vibration 279 (2005) 857–936.
[4] W.D. Iwan, A distributed-element model for hysteresis and its steady-state dynamic response, ASME Journal of Applied Mechanics 33 (1966) 893–900.
[5] P.R. Dahl, Solid friction damping of mechanical vibrations, AIAA Journal 14 (1976) 1675–1682.
[6] K.C. Valanis, A Theory of visco-plasticity without a yield surface, Archives of Mechanics 23 (1971) 171–191.
[7] L. Gaul, J. Lenz, Nonlinear dynamics of structures assembled by bolted joints, Acta Mechanica 125 (1997) 169–181.
[8] J. Swevers, F. Al-Bender, C.G. Ganesman, T. Prajogo, An integrated friction model structure with improved pre-sliding behavior for accurate friction compensation, IEEE Transactions on Automatic Control 45 (2000) 675–686.
[9] V. Lampaert, J. Swevers, F. Al-Bender, Modification of the Leuven integrated friction model structure, IEEE Transactions on Automatic Control 47 (2002) 683–687.
[10] D.A. Haessig, B. Friedland, On the modeling and simulation of friction, ASME Journal of Dynamic Systems, Measurement, and Control 113 (1991) 354–362.
[11] C.H. Canudas de Wit, K.J. Olsson, P. Astrom, A Lischinsky, new model for control of systems with friction, IEEE Transactions on Automantic Control 40 (1995) 419–425.
[12] L. Gaul, R. Nitsche, The role of friction in mechanical joints, Applied Mechanics Reviews 52 (2001) 93–106.
[13] D.J. Segalman, Modeling joint friction in structural dynamics, Structural Control Health Monitoring 13 (2006) 430–453.
[14] G. Gilardi, I. Sharf, Literature survey of contact dynamics modeling, Mechanism and Machine Theory 37 (2002) 1213–1239.
[15] E. Emaci, T. Nayfeh, A.F. Vakakis, Numerical and experimental study of nonlinear localization in a flexible structures with vibro-impacts, ZAMM 77 (1997) 527–541.
[16] F. Moon, S. Shaw, Chaotic vibrations of a beam with nonlinear boundary conditions, International Journal of Nonlinear Mechanics 18 (1983) 465–477.
[17] J. Knudsena, A.R. Massih, Dynamic stability of weakly damped oscillators with elastic impacts and wear, Journal of Sound and Vibration 263 (2003) 175–204.
[18] M.F.A. Azeez, A.F. Vakakis, Proper orthogonal decomposition (POD) of a class of vibroimpact oscillations, Journal of Sound and Vibration 240 (2001) 859–889.
[19] G. Kerschen, J.C. Golinval, K. Worden, Theoretical and experimental identification of a nonlinear beam, Journal of Sound and vibration 244 (2001) 597–613.
[20] E.F. Crawley, J.L. Sigler, M.C. Van Schoor, J. Marc, Prediction and measurement of damping in hybrid scaled space structure models, Report SSL, Space System Laboratory, Dept. of Aeronautical and Astronautical Engineering, MIT, 1988.
[21] K.H. Hunt, F.R.E. Crossley, Coefficient of restitution interpreted as damping in vibro-impact, Journal of Applied Mechanics 42 (1975) 440–445.
[22] S. Dubowsky, F. Freudenstein, Dynamic analysis of mechanical systems with clearances––Part 1: Formation of dynamical model, Journal of Engineering for Industry 93 (1971) 305–309.
[23] M.A. Veluswami, F.R.E. Crossley, Multiple impacts of a ball between two plates, Part 1: Some experimental observations, Journal of Engineering for Industry 97 (1975) 820–827.
[24] M.A. Veluswami, F.R.E. Crossley, Multiple impacts of a ball between two plates, Part 2: Some mathematical modeling, Journal of Engineering for Industry 97 (1975) 828–835.
[25] R.C. Azar, F.R.E. Crossley, Digital simulation of impact phenomenon in spur gear systems, Journal of Engineering for Industry 99 (1977) 792–798.
[26] C. Padmanabhan, R. Singh, Dynamics of a piecewise nonlinear system subject to dual harmonic excitation using parametric continuation, Journal of Sound and Vibration 184 (1995) 767–799.
[27] X. Ma, A. Berger, A. Vakakis, Identification of bolted joints through laser vibrometry, Journal of Sound and Vibration 246 (2001) 441–460.
[28] S. Folkman, B. Ferney, J. Bingham, J. Dutson, Friction and impact damping in a truss using pinned joints, Dynamics with Friction: Modeling, Analysis and Experiment, Part I, 1996, pp.137–168.
[29] W. Szemplinska-Stupnicka, The modified single mode method in the investigations of the resonant vibrations of nonlinear systems, Journal of Sound and Vibration 65 (1979) 475–489.
[30] W. Szemplinska-Stupnicka, Nonlinear normal modes and generalized Ritz method in the problems of vibrations of nonlinear elastic continuous systems, International Journal of Nonlinear Mechanics 18 (1983) 149–165.

[31] S. Perinpanayagam, D. Robb, D.J. Ewins, J.Moreno Barragan, Nonlinearities in an aero-engine structure: From test to design, International Conference on Modal Analysis, Noise and Vibration Engineering (2005) 3167–3181.
[32] S.F. Masri, J.P. Caffrey, T.K. Caughey, A.W. Smyth, A.G. Chassiakos, Identification of the state equation in complex nonlinear systems, International Journal of Nonlinear Mechanics 39 (2004) 1111–1127.
[33] K. Worden, G.R. Tomlinson, Nonlinearity in Structural Dynamics: Detection, Identification and Modeling., Institute of Physics Publishing, Bristol and Philadelphia, 2001.
[34] J.M.T. Thomson, H.B. Stewart, Nonlinear Dynamics and Chaos., Wiley & Sons, New York, 1986.